# Floquet Anderson localization of two interacting discrete time quantum walks

Merab Malishava,[1,2] Ihor Vakulchyk,[1,2] Mikhail Fistul,[1,3] and Sergej Flach[1]
[1]*Center for Theoretical Physics of Complex Systems, Institute for Basic Science (IBS), Daejeon 34126, Korea*
[2]*Basic Science Program, Korea University of Science and Technology (UST), Daejeon 34113, Korea*
[3]*Russian Quantum Center, National University of Science and Technology MISIS, 119049 Moscow, Russia*

(Received 27 November 2019; revised manuscript received 13 March 2020; accepted 16 March 2020; published 8 April 2020)

We study the interplay of two interacting discrete time quantum walks in the presence of disorder. Each walk is described by a Floquet unitary map defined on a chain of two-level systems. Strong disorder induces a novel Anderson localization phase with a gapless Floquet spectrum and one unique localization length $\xi_1$ for all eigenstates for noninteracting walks. We add a local contact interaction which is parametrized by a phase shift $\gamma$. A wave packet is spreading subdiffusively beyond the bounds set by $\xi_1$ and saturates at a new length scale $\xi_2 \gg \xi_1$. In particular we find $\xi_2 \sim \xi_1^{1.2}$ for $\gamma = \pi$. We observe a nontrivial dependence of $\xi_2$ on $\gamma$, with a maximum value observed for $\gamma$ values which are shifted away from the expected strongest interaction case $\gamma = \pi$. The novel Anderson localization regime indicates violation of single parameter scaling for both interacting and noninteracting walks.

DOI: 10.1103/PhysRevB.101.144201

## I. INTRODUCTION

Anderson localization (AL) [1–4] established that in the presence of uncorrelated on-site random potential, all eigenstates are exponentially localized in one and two dimensions. In three dimensions there is an energy mobility edge separating localized and delocalized eigenstates. The localization length $\xi_1$ is determined by many parameters such as eigenstate energy, hopping integrals between adjacent sites, and the amplitude of the random potential, as obtained for different lattices and various types of random potentials [4]. AL results in a strong suppression of transport in low-dimensional systems [1,4]. AL was observed experimentally in a variety of condensed matter and optical systems [3,5–9].

The challenging study of the interplay of interaction and disorder leads to a number of unexpected results for the localization properties of many particles eigenstates. This problem is relevant for understanding the many-body localization (MBL), a phenomenon of suppression of transport due to disorder in systems with macroscopic numbers of particles. MBL transition from ergodic to localized dynamic phases happen at certain values of the interaction strength and disorder rate ratios due to competing interplay between those two effects [10,11]. The minimal setup with two interacting particles (TIPs) can be considered as a building stone of the formation of MBL. The seemingly simplest case of TIPs in one space dimension was analyzed in an impressive set of publications [12–24]. For uncorrelated disorder the TIPs localization length $\xi_2$ is assumed to be finite, with the main questions addressing the way $\xi_2$ scales with $\xi_1$ in the limit of weak disorder [12–22], and the nature of the observed subdiffusive wave packet spreading on length scales $\xi_1 \ll L \ll \xi_2$ [23,24]. The lack of analytical results stresses the need for computational studies. However, in all above cases, there are limits set by the size of the system (in particular for diagonalization routines due to immense Hilbert space dimensions), the largest evolution times obtained through direct integrations of time-dependent Schrödinger equations with continuous time variables, and the energy dependence of the localization length $\xi_1$.

An interesting alternative platform is Floquet unitary maps on two-level system networks known as *discrete-time quantum walks* (DTQWs). DTQWs were introduced for quantum computing purposes [25–28]. A classical analog, (classical) random walks are used as a basis in multiple best performing classical algorithms, for example density of states calculation [29]. This inspired research of DTQW as a tool for quantum computing, with successful examples of significant speed-ups, for example quantum NAND trees evaluation [30]. Recently they have been used to study some numerically challenging complex problems of condensed matter physics, e.g., lattice Dirac transport [31], topological phases [32,33], Anderson localization [34–36], and nonlinear transport in ordered and disordered lattices supporting flat bands [37,38]. Note that the resulting Floquet Anderson localization is proven analytically for a whole range of different cases, including those where the eigenvalue spectrum is dense, homogeneous, and gapless, and the localization length $\xi_1$ is governing all random eigenstates independent of their eigenvalues [35]. We stress that DTQWs are particular examples of a Floquet driven quantum lattice, and, therefore, apply to studies of AL under nonequilibrium or simply infinite temperature conditions in an elegant and simple way as compared to the approach defined by time-periodic Hamiltonian systems (see, e.g., [39]). DTQWs have been implemented in various condensed matter and optics setups, see, e.g., [40–43].

Stefanak *et al.* [44] and Ahlbrecht *et al.* [45] proposed an extension of the single particle DTQW to two interacting DTQWs using a local contact interaction which is parametrized by a phase shift $\gamma$. We use this Hubbard-like

 

interaction and consider two interacting disordered discrete time quantum walks (TIWs). Using direct numerical simulations, we compute the time-dependent spreading of the TIWs wave packet and its dependence on the angle $\xi_1$, and the strength of the interaction $\gamma$. The computational evolution of wave functions for Hamiltonian systems involves the need to control accumulating errors due to the discretization of the continuous time variable. DTQWs do not require such approximations making them superior when it comes to long time evolutions.

The paper is organized as follows: in Sec. II we first present the model for a single one-dimensional DTQW. We then extend the model to two interacting DTQWs. In Sec. III we present the computational details and measures used for the study of the time evolution of two interacting DTQWs. In Sec. IV we present the numerical results, and discuss them. Section V provides the conclusions.

## II. MODELS

We consider the dynamics of a single quantum particle with an internal spinlike degree of freedom on a one-dimensional lattice [25–28,33,35,46,47]. Such a system is characterized by a two-component wave function $|\Psi(t)\rangle$ defined on a discrete chain of $N$ sites. The wave function is embedded in a $2N$-dimensional Hilbert space:

$$\begin{aligned}|\Psi(t)\rangle &= \sum_{n=1}^{N}\sum_{\alpha=\pm}\psi_n^{\alpha}(t)\,|\alpha\rangle\otimes|n\rangle \\ &= \sum_{n=1}^{N}[\psi_n^{+}(t)\,|+\rangle+\psi_n^{-}(t)\,|-\rangle]\otimes|n\rangle\,, \end{aligned} \tag{1}$$

where $|\alpha\rangle = |\pm\rangle$ are basis vectors of *local two-level systems*, $|n\rangle$ are basis vectors in a *one-dimensional coordinate space*, and $\psi_n^{\alpha}$ are the wave function amplitudes. The Floquet time evolution of the system is realized by means of a unitary map involving coin $\hat{C}$ and shift $\hat{S}$ operators:

$$|\Psi(t+1)\rangle = \hat{S}\hat{C}\,|\Psi(t)\rangle\,. \tag{2}$$

The coin operator $\hat{C}$ is a unitary matrix given by [35]

$$\hat{C} = \sum_{n=1}^{N}\hat{c}_n\otimes|n\rangle\,\langle n|\,, \tag{3}$$

with local unitary coin operators $\hat{c}_n$,

$$\hat{c}_n = e^{i\varphi_n}\begin{pmatrix} e^{i\varphi_{1,n}}\cos\theta_n & e^{i\varphi_{2,n}}\sin\theta_n \\ -e^{-i\varphi_{2,n}}\sin\theta_n & e^{-i\varphi_{1,n}}\cos\theta_n\end{pmatrix}, \tag{4}$$

which are parametrized by four spatially dependent angles $\theta_n$, $\varphi_n$, $\varphi_{1,n}$, and $\varphi_{2,n}$. Such local coin operators can be implemented in various experimental setups through, e.g., a periodic sequence of effective magnetic field pulses [40–43].

As it was shown in Ref. [35], the angle $\varphi_n$ is related to a potential energy, the angles $\varphi_{1,n}$ and $\varphi_{2,n}$ to an external and internal magnetic flux, respectively, and the angle $\theta_n$ to a local kinetic energy or hopping. In this work we intend to generalize the corresponding problem of two interacting particles in a one-dimensional tight-binding chain with uncorrelated disorder. Therefore, we choose $\varphi_{1,n} = \varphi_{2,n} = 0$ and $\theta_n \equiv \theta$, which

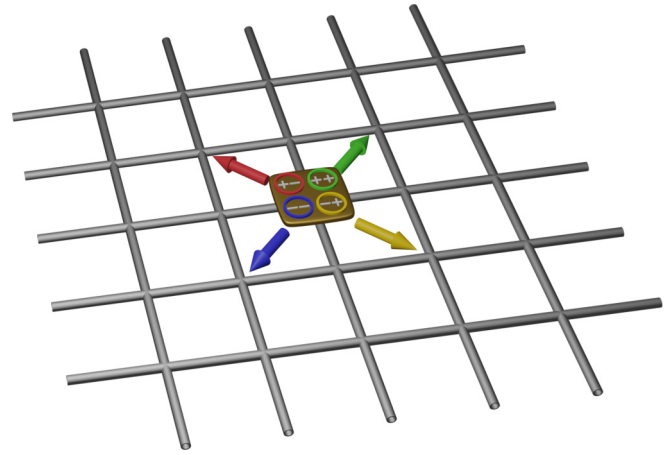

FIG. 1. A schematic view of the TIW. The four components of the wave function on each site of a square lattice are shifted in different directions indicated by the arrows.

simplifies the local coins $\hat{c}_n$ in (4) to

$$\hat{c}_n = e^{i\varphi_n}\begin{pmatrix}\cos\theta & \sin\theta \\ -\sin\theta & \cos\theta\end{pmatrix}. \tag{5}$$

The spatial local disorder will be introduced through the angles $\varphi_n$ [35]. This particular choice of disorder resembles a random on-site potential of the original Anderson model [1].

The shift operator $\hat{S}$ in Eq. (2) couples neighboring sites by shifting all the $\psi_n^{+}$ components one step to the right, and all the $\psi_n^{-}$ components to the left:

$$\hat{S} = \sum_{n}|n\rangle\,\langle n+1|\otimes|-\rangle\,\langle-| \;+\; |n\rangle\,\langle n-1|\otimes|+\rangle\,\langle+|\,. \tag{6}$$

This completes the definition of a single particle discrete-time quantum walk [25–28,33,35,46,47].

We extend the above single particle walk to two interacting discrete time quantum walks (TIWs) in analogy to the extension of a single quantum particle in the Anderson model to two interacting particles:

$$|\Psi(t)\rangle = \sum_{i,j=1}^{N}\sum_{\alpha,\beta=\pm}\psi_{ij}^{\alpha\beta}(t)\,|\alpha,\beta\rangle\otimes|i,j\rangle\,. \tag{7}$$

The wave function $|\Psi(t)\rangle$ is embedded in a $4N^2$-dimensional Hilbert space where $|\alpha,\beta\rangle$ are basis vectors of two local two-level systems, and $|i,j\rangle$ are basis vectors in a two-dimensional square lattice. The TIW evolution is obtained through a product of a TIW coin $\hat{W}$, shift $\hat{T}$, and interaction $\hat{G}$ operators acting on the wave function (see Fig. 1):

$$|\Psi(t+1)\rangle = \hat{T}\hat{W}\hat{G}\,|\Psi(t)\rangle\,. \tag{8}$$

The coin $\hat{W}$ and shift $\hat{T}$ operators are tensor products of the corresponding single particle operators:

$$\hat{W} = \hat{C}\otimes\hat{C}, \quad \hat{T} = \hat{S}\otimes\hat{S}. \tag{9}$$

In the absence of interaction $\hat{G} = \mathbb{1}$ they describe the evolution of two independent single particle DTQWs. The local Hubbard-like contact interaction between the two DTQWs

was introduced in Ref. [45] as

$$\hat{G} = \mathbb{1}_c \otimes \mathbb{1}_p + (e^{i\gamma} - 1)\mathbb{1}_c \otimes \hat{N}, \tag{10}$$

where $\gamma$ is the interaction strength parameter. $\hat{N} = \sum_i |i,i\rangle\langle i,i|$ is a projector on the diagonal of the coordinate space, $\mathbb{1}_c$ is the $4 \times 4$ unity matrix in the coin space, and $\mathbb{1}_p$ is the $N^2 \times N^2$ unity matrix in the position space. Note that $\gamma = 0$ corresponds to two noninteracting DTQWs.

## III. ANDERSON LOCALIZATION

The local disorder is introduced through uncorrelated random values of the angle $\varphi_n$. For the disorder strength $0 \leqslant W \leqslant 2\pi$, a set of $\varphi_n$ is independently drawn from a uniform distribution of $[-W/2, W/2]$.

### A. Single particle DTQW

As it was shown in Ref. [35], all eigenstates of the single particle DTQW are exponentially localized and characterized by a localization length $\xi_1$, in full analogy to Anderson localization for Hamiltonian single particle systems [1]. The single particle DTQW possesses two distinct limiting parameter cases for which $\xi_1 \to \infty$. The first is obtained for $W \to 0$, again in full analogy with Hamiltonian systems. The DTQW eigenvalues form a band spectrum and are located on the unit circle [35], which is in general gapped for $W \to 0$. Consequently the localization length $\xi_1$ is a function of the eigenvalue and different for different eigenstates, reaching its largest value in the center of the above bands. The second parameter case is unique for Floquet Anderson systems and is obtained for the case of *strongest* disorder $W = \pi$. The DTQW spectrum is now dense, homogeneous, and gapless on the unit circle, with all eigenstates having the same localization length irrespective of their eigenvalue [35]:

$$\xi_1 = -\frac{1}{\ln(|\cos\theta|)}. \tag{11}$$

The limit $\xi_1 \to \infty$ is obtained by varying the hopping angle $\theta \to 0$. We are not aware of a similar regime for Hamiltonian systems. In the following, we will study the TIW in that novel regime.

### B. TIW

We will follow the time evolution of a TIW wave function starting from the initial state

$$|\Psi(t=0)\rangle = \frac{(|+,-\rangle + |-,+\rangle)}{\sqrt{2}} \otimes |N/2, N/2\rangle \tag{12}$$

for which the two single particle DTQWs are localized on the lattice site $N/2$ where the TIW interaction is present. The system size $N$ varies from 5000 up to 25 000, such that the spreading wave packet does not reach the edges in order to exclude finite system size corrections. We perform a direct numerical propagation of (8) up to $t_{\max}$ which varies from $10^4$ for the $\gamma = 0$ to $10^6$ for nonzero interaction strength values.

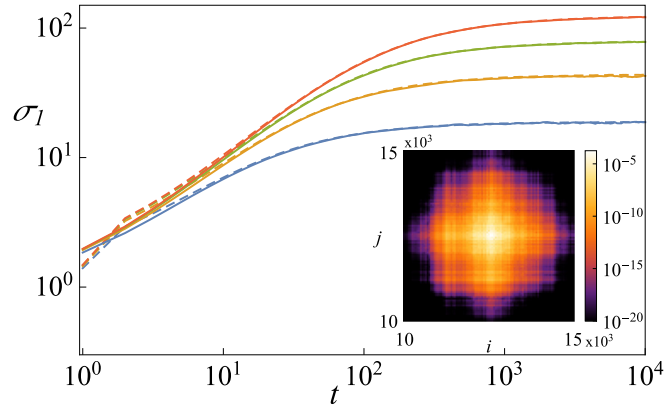


FIG. 2. $\sigma_1(t)$ for $\gamma = 0$ (solid lines, 100 disorder realizations) and $\sigma_{\rm sp}(t)$ (dashed lines, average over $10^4$ disorder realizations). $\theta = \pi/8, \pi/12, \pi/16, \pi/20$ from bottom to top. Here $N = 5000$ for $\theta = \pi/8, \pi/12$ and $N = 25\,000$ for $\theta = \pi/16, \pi/20$. Inset: Snapshot of the probability distribution $p_{ij}(t = 10^4)$ for $\theta = \pi/20$.

We follow the wave function probability distribution in coordinate space

$$p_{ij}(t) = \sum_{\alpha,\beta=\pm} \left|\psi_{ij}^{\alpha\beta}\right|^2. \tag{13}$$

To assess TIW localization length scales we will project $p_{ij}$ in three different ways onto a one-dimensional coordinate space and compute the standard deviation of a probability distribution vector $\{v_i\}$ (see, e.g., [23,24]):

$$\sigma[\{v_i\}] = \left(\sum_i i^2 v_i - \left(\sum_i i v_i\right)^2\right)^{1/2}. \tag{14}$$

*Measure 1: projection on a one particle space*: we define $v_i = \sum_j p_{ij}(t)$, substitute it in (14) and obtain $\sigma_1(t)$.

*Measure 2: projection on the space of the center mass motion*: we define $v_i = \sum_j p_{i,j-i}(t)$, substitute it in (14) and obtain $\sigma_\parallel(t)$.

*Measure 3: projection on the space of (relative) distance between particles*: we define $v_i = \sum_j p_{i,i+j}(t)$, and substitute it in (14) and obtain $\sigma_\perp$.

In addition to the above three TIW length scales $\sigma_1, \sigma_\parallel, \sigma_\perp$ we also define a length scale $\sigma_{\rm sp}$ which follows from the numerical simulation of a single particle DTQW. We define $v_i = |\psi_i^+(t)|^2 + |\psi_i^-(t)|^2$, substitute it in (14), and obtain $\sigma_{\rm sp}$.

In the presence of Anderson localization, all the above length scales are expected to grow in time and saturate at some finite values for $t \to \infty$. For the single particle DTQW we expect $\sigma_{\rm sp}(t \to \infty) \sim \xi_1$. For the noninteracting TIW case $\gamma = 0$ we expect the distribution $p_{ij}(t \to \infty)$ to have fourfold discrete rotational symmetry (see, e.g., inset in Fig. 2). It follows $\sigma_1 \approx \sigma_\parallel \approx \sigma_\perp \approx \sigma_{\rm sp} \sim \xi_1$. However, for $\gamma \neq 0$ the two walks are expected to be able to travel beyond the limits set by $\sigma_{\rm sp}$ and $\xi_1$ as long as their two coordinates are close enough such that $|i - j| < \xi_1$. This is in analogy to two interacting particles in Hamiltonian settings. The interaction is introducing nonzero matrix elements between the Anderson eigenstates of the noninteracting system which leads to an effective internal degree of freedom of two walks (or particles)

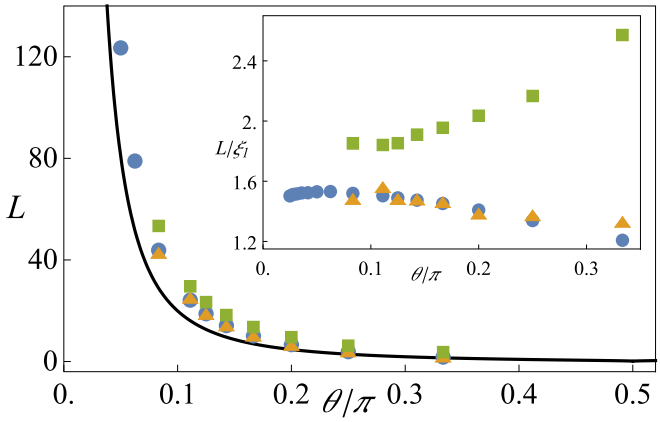


FIG. 3. Various length scales $L$ versus $\theta$: $\xi_1$ (solid line), $\sigma_{\rm sp}(t_f)$ (blue circles), $\sigma_1(t_f)$ (red triangles), $P$ (green squares). Here $t_f = 2 \times 10^4$, $\gamma = 0$. Inset: $\sigma_{\rm sp}/\xi_1$, $\sigma_1/\xi_1$, and $P/\xi_1$ as a function of the angle $\theta$. Results have been averaged over $10^4$ disorder realizations for $\sigma_{\rm sp}(t_f)$, 100 realizations for $\sigma_1(t_f)$ and 5000 eigenstates for $P$. Error bars are smaller than the marker size.

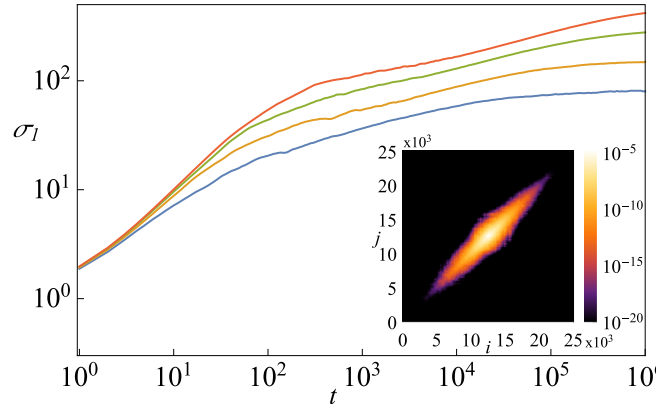


FIG. 4. Time evolution of $\sigma_1$ of a TIW for different values of $\theta = \pi/8, \pi/12, \pi/16, \pi/20$ from bottom to top. Here $\gamma = \pi$ and $N = 25\,000$. Inset: Snapshot of the probability distribution $p_{ij}$ for $\theta = \pi/20$ at $t = 10^6$, showing strongly anisotropic wave packet spreading.

which form a weakly bound state. Consequently the distribution $p_{ij}(t \to \infty)$ should elongate along the diagonal $i = j$ and reduce its symmetry to a twofold rotational symmetry (see, e.g., inset in Fig. 4). It follows $\sigma_1 \approx \sigma_\parallel \equiv \xi_2, \sigma_\perp \approx \sigma_{\rm sp} \sim \xi_1$, and $\xi_2 \gg \xi_1$. The TIW is therefore characterized by two length scales $\xi_2$ and $\xi_1$.

## IV. COMPUTATIONAL RESULTS

### A. $\gamma = 0$

The time dependence $\sigma_1(t)$ (averaged over 100 disorder realizations) is shown in Fig. 2 for various values of the hopping angle $\theta$ with solid lines. We observe the expected saturation of $\sigma_1$ for large evolution times $t = 10^4$. The wave function probability distribution $p_{ij}(t = 10^4)$ is shown in the inset of Fig. 2 for $\theta = \pi/20$. It shows the above discussed fourfold discrete rotational symmetry. In addition we plot the time dependence of $\sigma_{\rm sp}(t)$ with dashed lines, which are averaged over $10^4$ disorder realizations and nicely follow the corresponding $\sigma_1(t)$ curves.

A first nontrivial test is the comparison of $\xi_1$ with $\sigma_{sp}(t \to \infty)$ and $\sigma_1(t \to \infty)$ for $\gamma = 0$. While we expect $\sigma_{\rm sp} \approx \sigma_1$, the connection between $\xi_1$ and $\sigma_{sp}$ is far from obvious. The Hamiltonian case is known to obey the single parameter scaling property [48], which implies in our case $\xi_1 \sim \sigma_{\rm sp}$. In Fig. 3 we compare the localization length $\xi_1$ (11) (solid line) with $\sigma_{sp}(t = 10^4)$ from Fig. 2 (blue circles) and $\sigma_1(t = 10^4)$ from Fig. 2 (red triangles) for different values of $\theta$. At a first glance the single parameter scaling seems to be satisfied, since the data symbols follow the analytical curve reasonably closely. However, the inset in Fig. 3 plots the corresponding ratios $\sigma_{\rm sp}/\xi_1$ and $\sigma_1/\xi_1$ versus $\theta$ which result in nonhorizontal curves and indicate a violation of the single parameter scaling hypothesis. To further test indications of the absence of the single parameter scaling property, we diagonalize the single particle DTQW numerically for a system size $N = 1500$, and obtain the participation numbers $P_\nu$ of all eigenfunctions $|\Psi\rangle_\nu$ as $1/P = \sum_{n=1}^{N} \sum_{\alpha=\pm} |\psi_n^\alpha|^4$. The average $P = \sum_\nu P_\nu/2N$ is plotted in Fig. 3 (green squares). We find that $P/\xi_1$ is varying with $\xi_1$, and even shows an opposite trend as compared to $\sigma_{\rm sp}/\xi_1$, possibly confirming the presence of a variety of different length scales in the problem.

At the same time, $\sigma_{\rm sp}$ closely follows $\sigma_1$, implying that any changes in $\sigma_1$ upon increasing the TIW interaction $\gamma$ away from $\gamma = 0$ are solely due to the interaction, and not due to measurement ambiguities.

### B. $\gamma = \pi$

Let us present the numerical analysis of the dynamics of the TIW for nonvanishing interaction $\gamma \neq 0$. The largest absolute value of the term $(e^{i\gamma} - 1)$ in (10) is obtained for $\gamma = \pi$, which we choose as our operational value in this section. We evolve a system of size $N = 25\,000$ up to time $t_{\rm max} = 10^6$. We follow the time dependence of the standard deviation $\sigma_1$ for various values of the angle $\theta$. These results are presented in Fig. 4 (solid lines). $\sigma_1(t)$ shows ballisticlike growth ($\sigma \propto t$) up to $\sigma_1 \sim \xi_1$ in analogy to the noninteracting case. During this first part of the dynamics, the wave packet spreads up to a length scale of the order of the single particle localization length $\xi_1$. At variance to the noninteracting case, the interacting dynamics continues beyond the limits set by the single particle DTQW Anderson localization. The corresponding growth of $\sigma_1$ with time is close to a subdiffusive one $\sigma \propto t^\alpha$ with $\alpha \leqslant 0.5$.

For $\theta = \pi/8$ and $\xi_1 \approx 12$ we observe saturation of $\sigma_1(t)$ at the largest computational time $t = 10^6$. For smaller values of $\theta$ and correspondingly for larger values of $\xi_1$, the saturation is shifted to larger time and spatial scales, and becomes barely visible for $\theta = \pi/20$ and $\xi_1 \approx 81$. Choosing larger system sizes, despite being necessary, turns hard due to CPU time and memory limitations. For practical purposes we therefore will present data which correspond to the largest evolution times.

In the inset of Fig. 4 we plot the probability distribution of wave function $p_{ij}(t = 10^6)$ for $\theta = \pi/20$. It shows a clear reduction to the twofold rotational symmetry which leads to the emergence of at least two different length scales $\sigma_\perp$ and $\sigma_\parallel \gg \sigma_\perp$ which characterize the width and elongation of the

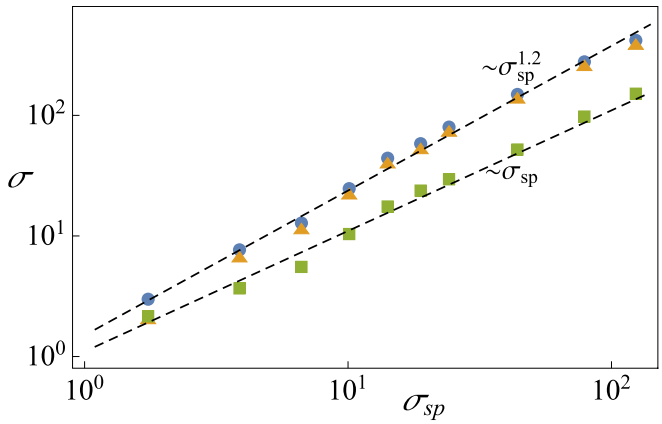


FIG. 5. Scaling of the TIW length scale $\sigma_\perp$ (green squares), $\sigma_\parallel$ (orange triangles), and $\sigma_1$ (blue circles) with the single particle DTQW length scale $\sigma_{sp}$. The corresponding values of $\theta$ vary between $\pi/20$ and $\pi/3$. Here $\gamma = \pi$ and $N = 25\,000$. Black dashed lines are algebraic fits.

cigarlike shape. The dependence of the new length scales on the single particle $\sigma_{sp}$ one is shown in Fig. 5. The width $\sigma_\perp \approx \sigma_{sp}$ demonstrates that the limit of relative distance on which the two single particle DTQW components of the TIW can propagate is set by $\sigma_{sp}$. However, the elongation $\sigma_\parallel$ shows a faster than linear growth with $\sigma_{sp}$. A simple power-law fit $\sigma_\parallel \approx \sigma_{sp}^\beta$ yields $\beta \approx 1.2$.

### C. Varying $\gamma$

Finally we study the impact of varying the interaction strength $\gamma$ for two different values of $\theta = \pi/8$ and $\theta = \pi/12$ in Fig. 6. In order to avoid disorder realization induced fluctuations, we evolve the wave packet up to $t = 2 \times 10^5$ (which is sufficient for the chosen $\theta$ values) and average over ten disorder realizations. We first discuss the data for the width $\sigma_\perp$. Since we concluded that $\sigma_\perp \approx \sigma_{sp}$ is a single particle DTQW length scale, it should not depend on the value of $\gamma$. Indeed, the computational data demonstrate this very clearly. At the same time, the elongation scale $\sigma_\parallel$, with respect to $\sigma_1$, should strongly depend on $\gamma$. Again, the computational data in Fig. 6 demonstrate this very clearly. The curves $\sigma_{\parallel,1}(\theta)$ show a clear maximum at $\gamma_m(\theta)$. Surprisingly, $\gamma_m \neq \pi$, with a weak but observable dependence on $\theta$. Therefore the value $\gamma = \pi$ is in general not corresponding to the case of strongest enhancement of the TIW localization length. Possibly there is a hidden symmetry in the TIW problem at $\gamma = \pi$ whose violation for $\gamma \neq \pi$ might lead to an enhancement of the localization length.

## V. CONCLUSION AND OUTLOOK

We analyzed the interplay of disorder and interaction in the Floquet Anderson localization problem of two interacting discrete time quantum walks. The single particle DTQW is described by a Floquet unitary map defined on a chain of two-level systems. Despite the action of strong disorder in one of the Floquet unitary map parameters, the resulting novel Anderson localization phase is characterized by a gapless Floquet spectrum and one unique localization length $\xi_1$ for

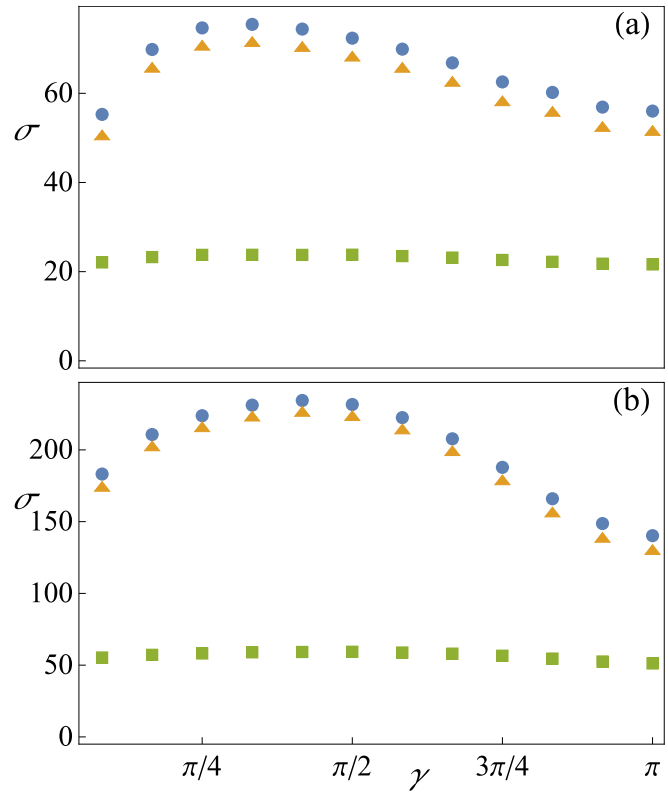


FIG. 6. $\sigma_1$ (blue circles), $\sigma_\parallel$ (orange triangles), $\sigma_\perp$ (green squares) as functions of the interaction parameter $\gamma$. (a) $\theta = \pi/8$. (b) $\theta = \pi/12$. Results have been averaged over ten disorder realizations. Error bars are smaller than the marker size.

all single particle eigenstates. The ratio of the participation number of the eigenstates $P$ over $\xi_1$ is not constant, indicating a violation of the usually expected single parameter scaling regime as known for Hamiltonian disordered systems. We add a local contact interaction, which is parametrized by a phase shift $\gamma$. A wave packet is spreading subdiffusively beyond the bounds set by $\xi_1$ and saturates at a new length scale $\xi_2 \gg \xi_1$. For the assumed strongest interaction case $\gamma = \pi$ we identify a new length scale $\xi_2 \gg \xi_1$ which follows $\xi_2 \sim \xi_1^{1.2}$. We observe a nontrivial dependence of $\xi_2$ on $\gamma$, with a maximum value observed for $\gamma$ values which are shifted away from the expected strongest interaction case $\gamma = \pi$. We currently lack an understanding of this intriguing fact, which has to be addressed in future work. In the absence of interaction $\gamma = 0$ we observe indications of the violation of the single parameter scaling. We can only speculate on possible reasons for this observation. Are we not close enough to the asymptotic regime of very large localization length? Is the observation caused by the fact that the localization length diverges, but the eigenstates do not restore a (translational) symmetry in real space and stay disordered? The explanation of this surprising observation is another interesting topic to be addressed in future work.

## ACKNOWLEDGMENT

This work was supported by the Institute for Basic Science, Project Code (Grant No. IBS-R024-D1).

[1] P. W. Anderson, Absence of diffusion in certain random lattices, Phys. Rev. **109**, 1492 (1958).

[2] P. A. Lee and T. V. Ramakrishnan, Disordered electronic systems, Rev. Mod. Phys. **57**, 287 (1985).

[3] B. Kramer and A. MacKinnon, Localization: Theory and experiment, Rep. Prog. Phys. **56**, 1469 (1993).

[4] I. Lifshits, S. Gredeskul, and L. Pastur, *Introduction to the Theory of Disordered Systems* (Wiley, New York, 1988).

[5] Y. Lahini, A. Avidan, F. Pozzi, M. Sorel, R. Morandotti, D. N. Christodoulides, and Y. Silberberg, Anderson Localization and Nonlinearity in One-Dimensional Disordered Photonic Lattices, Phys. Rev. Lett. **100**, 013906 (2008).

[6] J. Billy, V. Josse, Z. Zuo, A. Bernard, B. Hambrecht, P. Lugan, D. Clément, L. Sanchez-Palencia, P. Bouyer, and A. Aspect, Direct observation of Anderson localization of matter waves in a controlled disorder, Nature (London) **453**, 891 (2008).

[7] G. Roati, C. D'Errico, L. Fallani, M. Fattori, C. Fort, M. Zaccanti, G. Modugno, M. Modugno, and M. Inguscio, Anderson localization of a non-interacting Bose-Einstein condensate, Nature (London) **453**, 895 (2008).

[8] M. Störzer, P. Gross, C. M. Aegerter, and G. Maret, Observation of the Critical Regime Near Anderson Localization of Light, Phys. Rev. Lett. **96**, 063904 (2006).

[9] T. Schwartz, G. Bartal, S. Fishman, and M. Segev, Transport and Anderson localization in disordered two-dimensional photonic lattices, Nature (London) **446**, 52 (2007).

[10] A. Pal and D. A. Huse, Many-body localization phase transition, Phys. Rev. B **82**, 174411 (2010).

[11] D. A. Abanin, E. Altman, I. Bloch, and M. Serbyn, Colloquium: Many-body localization, thermalization, and entanglement, Rev. Mod. Phys. **91**, 021001 (2019).

[12] D. L. Shepelyansky, Coherent Propagation of Two Interacting Particles in a Random Potential, Phys. Rev. Lett. **73**, 2607 (1994).

[13] P. Jacquod, D. L. Shepelyansky, and O. P. Sushkov, Breit-Wigner Width for Two Interacting Particles in a One-Dimensional Random Potential, Phys. Rev. Lett. **78**, 923 (1997).

[14] Y. Imry, Coherent propagation of two interacting particles in a random potential, Europhys. Lett. **30**, 405 (1995).

[15] R. A. Römer and M. Schreiber, No Enhancement of the Localization Length for Two Interacting Particles in a Random Potential, Phys. Rev. Lett. **78**, 515 (1997).

[16] F. von Oppen, T. Wettig, and J. Müller, Interaction-Induced Delocalization of Two Particles in a Random Potential: Scaling Properties, Phys. Rev. Lett. **76**, 491 (1996).

[17] P. H. Song and F. von Oppen, General localization lengths for two interacting particles in a disordered chain, Phys. Rev. B **59**, 46 (1999).

[18] K. Frahm, A. Müller-Groeling, J.-L. Pichard, and D. Weinmann, Scaling in interaction-assisted coherent transport, Europhys. Lett. **31**, 169 (1995).

[19] K. M. Frahm, Eigenfunction structure and scaling of two interacting particles in the one-dimensional Anderson model, Eur. Phys. J. B **89**, 115 (2016).

[20] D. O. Krimer and S. Flach, Statistics of wave interactions in nonlinear disordered systems, Phys. Rev. E **82**, 046221 (2010).

[21] D. O. Krimer, R. Khomeriki, and S. Flach, Two interacting particles in a random potential, JETP Lett. **94**, 406 (2011).

[22] M. Ortuño and E. Cuevas, Localized to extended states transition for two interacting particles in a two-dimensional random potential, Europhys. Lett. **46**, 224 (1999).

[23] M. V. Ivanchenko, T. V. Laptyeva, and S. Flach, Quantum chaotic subdiffusion in random potentials, Phys. Rev. B **89**, 060301(R) (2014).

[24] I. I. Yusipov, T. V. Laptyeva, A. Y. Pirova, I. B. Meyerov, S. Flach, and M. V. Ivanchenko, Quantum subdiffusion with two- and three-body interactions, Eur. Phys. J. B **90**, 66 (2017).

[25] D. Aharonov, A. Ambainis, J. Kempe, and U. Vazirani, Quantum walks on graphs, in *Proceedings of the Thirty-Third Annual ACM Symposium on Theory of Computing* (ACM, New York, United States, 2001), pp. 50–59.

[26] Y. Aharonov, L. Davidovich, and N. Zagury, Quantum random walks, Phys. Rev. A **48**, 1687 (1993).

[27] J. Kempe, Quantum random walks: An introductory overview, Contemp. Phys. **44**, 307 (2003).

[28] B. Tregenna, W. Flanagan, R. Maile, and V. Kendon, Controlling discrete quantum walks: Coins and initial states, New J. Phys. **5**, 83 (2003).

[29] F. Wang and D. P. Landau, Efficient, Multiple-Range Random Walk Algorithm to Calculate the Density of States, Phys. Rev. Lett. **86**, 2050 (2001).

[30] E. Farhi, J. Goldstone, and S. Gutmann, A quantum algorithm for the Hamiltonian nand tree, Theor. Comput. **4**, 169 (2008).

[31] C. Chandrashekar, Two-component Dirac-like Hamiltonian for generating quantum walk on one-, two-, and three-dimensional lattices, Sci. Rep. **3**, 2829 (2013).

[32] T. Kitagawa, M. S. Rudner, E. Berg, and E. Demler, Exploring topological phases with quantum walks, Phys. Rev. A **82**, 033429 (2010).

[33] H. Obuse and N. Kawakami, Topological phases and delocalization of quantum walks in random environments, Phys. Rev. B **84**, 195139 (2011).

[34] T. Chattaraj and R. V. Krems, Effects of long-range hopping and interactions on quantum walks in ordered and disordered lattices, Phys. Rev. A **94**, 023601 (2016).

[35] I. Vakulchyk, M. V. Fistul, P. Qin, and S. Flach, Anderson localization in generalized discrete-time quantum walks, Phys. Rev. B **96**, 144204 (2017).

[36] L. A. Toikka, Disorder-induced two-body localized state in interacting quantum walks, Phys. Rev. B **101**, 064202 (2020).

[37] I. Vakulchyk, M. V. Fistul, and S. Flach, Wave Packet Spreading with Disordered Nonlinear Discrete-Time Quantum Walks, Phys. Rev. Lett. **122**, 040501 (2019).

[38] I. Vakulchyk, M. Fistul, Y. Zolotaryuk, and S. Flach, Almost compact moving breathers with fine-tuned discrete time quantum walks, Chaos **28**, 123104 (2018).

[39] R. Ducatez and F. Huveneers, *Anderson Localization for Periodically Driven Systems* (Springer, Berlin, 2017), pp. 2415–2446.

[40] Y. Makhlin, G. Schön, and A. Shnirman, Quantum-state engineering with Josephson-junction devices, Rev. Mod. Phys. **73**, 357 (2001).

[41] B. C. Sanders, S. D. Bartlett, B. Tregenna, and P. L. Knight, Quantum quincunx in cavity quantum electrodynamics, Phys. Rev. A **67**, 042305 (2003).

[42] T. Di, M. Hillery, and M. S. Zubairy, Cavity qed-based quantum walk, Phys. Rev. A **70**, 032304 (2004).

[43] M. Karski, L. Förster, J.-M. Choi, A. Steffen, W. Alt, D. Meschede, and A. Widera, Quantum walk in position space with single optically trapped atoms, Science **325**, 174 (2009).

[44] M. Štefaňák, S. Barnett, B. Kollár, T. Kiss, and I. Jex, Directional correlations in quantum walks with two particles, New J. Phys. **13**, 033029 (2011).

[45] A. Ahlbrecht, A. Alberti, D. Meschede, V. B. Scholz, A. H. Werner, and R. F. Werner, Molecular binding in interacting quantum walks, New J. Phys. **14**, 073050 (2012).

[46] S. E. Venegas-Andraca, Quantum walks: A comprehensive review, Quant. Info. Proc. **11**, 1015 (2012).

[47] C. M. Chandrashekar, R. Srikanth, and R. Laflamme, Optimizing the discrete time quantum walk using a SU(2) coin, Phys. Rev. A **77**, 032326 (2008).

[48] A. MacKinnon and B. Kramer, The scaling theory of electrons in disordered solids: additional numerical results, Z. Phys. B: Condens. Matter **53**, 1 (1983).